

## A Multilayer Nanostructure for Linear Zone-Plate Applications\*

Chian Liu <sup>a)</sup>, R. Conley, A. T. Macrander, and J. Maser  
Experimental Facilities Division, Argonne National Laboratory, Argonne, IL 60439

H. C. Kang and G. B. Stephenson  
Center for Nanoscale Materials and Materials Science Division, Argonne National  
Laboratory, Argonne, IL 60439

We have prepared a multilayer nanostructure of 728 layers with thicknesses gradually increasing from 10 to ~58 nm according to the Fresnel zone-plate formula, for a total thickness of 12.43  $\mu\text{m}$ . The thickness difference between the neighboring layers varies monotonically from 0.0067 nm at the thin end to 1.2421 nm at the thick end. We have grown this nanostructure on Si(100) substrates using dc magnetron sputtering of  $\text{WSi}_2$  and Si targets with the power supplies controlled in constant-current, as well as constant-power, modes. The multilayers were subsequently sectioned and polished for hard x-ray nanofocusing experiments. For x-rays diffracted by each and every layer to add “in phase” at the primary focus, the layers need to be deposited precisely with the correct thicknesses. Layer thicknesses were checked with scanning electron microscope (SEM) images on zone-plate multilayers and x-ray reflectivity measurements on test periodic multilayers. The challenges and experiments for the growth of this type of thick depth-graded multilayer with a high accuracy of layer positioning will be presented.

<sup>a)</sup> Electronic mail: [cliu@aps.anl.gov](mailto:cliu@aps.anl.gov), phone: 630-252-9985, fax: 630-252-9303.

PACS: 81.15.Cd, 68.65.Ac, 41.50.th.

Keywords: magnetron sputter deposition, multilayers, x-ray optics.

\* This work is supported by the U. S. Department of Energy, under Contract No. W-31-109-ENG-38.

## 1. Introduction

Traditional zone plates are circular transmission gratings consisting of alternating transparent and opaque (or phase-shifting) rings. Each ring (or zone) is positioned so that the optical path from the zone plate to the primary focus differs by  $\lambda/2$  between consecutive zones, where  $\lambda$  is the x-ray wavelength. The optimum zone positions are given by the Fresnel zone formula [1-3]

$$r_n^2 = n\lambda f + n^2\lambda^2/4, \quad (1)$$

where  $r_n$  is the radius of the  $n$ th zone, and  $f$  is the focal length. The second term in Eq. (1) is a correction for spherical aberration and can be omitted when  $n\lambda \ll f$ . The width of the  $n$ th zone is  $(r_n - r_{n-1})$ . The focusing capability of a zone plate depends on the width of the outermost zone, the optical contrast between the alternating zones, and the accuracy of the zone placement. For optimized x-ray zone-plate materials, depths of several microns are typically required for efficient focusing of hard x-rays.

Traditional zone plates are fabricated using lithographic techniques. To achieve the required high aspect ratio of zone depth to width, a mask with the zone-plate pattern is first made using e-beam lithography, and x-ray lithography is then used with a thick resist and subsequent metal electroplating on silicon nitride membranes for zone-plate fabrication [4]. For efficient focusing of hard x-rays, one needs a very large aspect ratio. Tremendous progress has been made in this field, and very recently a spatial resolution of 60 nm was achieved for hard x-rays using zone plates with a 50 nm outermost zone width and 1  $\mu\text{m}$  zone depth with gold as the zone material [5,6]. However, as the desired zone width becomes smaller and zone depth larger, the manufacturing process becomes increasingly difficult.

An alternative approach to the fabrication of hard x-ray zone plates is the deposition and sectioning of multilayers. The techniques for producing x-ray multilayers were developed over 35 yrs ago [7]. The thickness of deposited films can be controlled in the angstrom range, much more precisely than the x-y positioning in a lithographic system. With slicing and polishing, large aspect ratios can easily be obtained. To date, sectioned, multilayer-coated wires have been used for zone plates [8,9]. However, the wires are not ideally round or smooth at the nanoscale, affecting the uniformity of zone positions. And also, when coating on a round wire, some oblique incidence of the sputter atoms is unavoidable, causing a shadowing effect and leading to film roughness [10]. These factors limit the achievable focusing capability of sputtered-sliced wires.

We have recently been exploring the fabrication of linear zone plates using sputtered-sliced multilayers grown on flat Si substrates [11-13]. As illustrated in Fig. 1, two identical planar multilayer sections would be assembled to form the two halves of a linear zone plate, to produce a focus in one dimension. The separation of the two halves allows them to be tilted at the optimum angle for high diffraction efficiency. Another pair rotated by 90° about the optical axis could be used to produce a point focus. Since the multilayer sections are assembled with the substrate side oriented away from the optical axis, the thinnest zones can be grown first, minimizing the impact of accumulated growth imperfections on zone-plate performance. We have prepared a multilayer of 728 layers of WSi<sub>2</sub> and Si with thicknesses gradually increasing from 10 to ~58 nm according to the Fresnel zone-plate formula, for a total thickness of 12.43 μm. Because of its unique advantages, WSi<sub>2</sub>/Si was selected as the multilayer system for linear zone-plate applications. Compared with the W/Si system, WSi<sub>2</sub>/Si has sharper interfaces and is

thermally more stable [14-16]. It has also been found that the layer thicknesses for W/Si multilayers do not extrapolate to zero at zero growth time while for WSi<sub>2</sub>/Si multilayers they do [17,18]. To deposit the thick zone-plate multilayers with accurate layer thicknesses, it is extremely important to have a stable system and be able to correct the growth rate accurately. Even though magnetron deposition is known to be very stable compared to other deposition techniques, small drifts in deposition rates due to a continuously changing erosion profile of the target are also known [19-21]. This drift in deposition rates becomes more serious for prolonged depositions. The growths of thick zone-plate multilayers provides an opportunity to study how the growth-rate changes at different growing stages. In addition to drifts due to changing target conditions, there are re-sputtering effects on the film caused by backscattered neutral Ar gas atoms from the targets. The re-sputtering yield may be enhanced for thin films of light elements when they are backed by heavy ones, causing complications in growth rate calibration [22, 23]. The re-sputtering effect is most significant for very thin films. For thick ones, the re-sputtering yield approaches the bulk value and is no longer a varying factor. For other factors affecting the growth rate, we have noticed a gradual decrease of discharge voltages with deposition time when a constant-current mode was used in the sputter-gun power supply. The falling flakes from the Si that deposit on the shielding masks above the sputter gun in our deposition system have also had an adverse influence on the growth rate. In this paper we compare multilayers grown with a constant-current control to that with a constant-power control of the power supplies, describe ways to overcome flaking problems, and present results of growth-rate drifts at different stages of zone-plate multilayer growth using SEM image analyses and x-ray reflectivity measurements.

## 2. Experiment

The multilayers were made by dc magnetron sputtering in our deposition facility, which consists of four large vacuum chambers, each 16 inches in diameter and 66 inches long. Three CTI model CT-8 cryo pumps and an Alcatel ADP 81 dry pump provide a base pressure of  $< 1 \times 10^{-8}$  Torr for the system. The substrates on a substrate holder were loaded on a carrier with the optical surface facing down and were alternately translated back and forth over two 3-inch-diameter planar sputter guns during deposition. The sputter guns were magnetically balanced. They were located in two 16-inch-diameter 12-inch-high wells, 15 inches apart, at the bottom side of the deposition chamber. They were surrounded by shield cans with only a shaped aperture open on the top. The opening at the center of the aperture is 46 mm. The substrates are  $12.5 \times 25 \times 1.5 \text{ mm}^3$  Si plates cut from Si(100) wafers. Multiple substrates can be loaded at different locations on a 60-inch-long substrate holder for different multilayer growths. The substrate-to-target distance was 107 mm, and there was no bias applied to the substrates. Laterally uniform depositions were achieved through the design of shaped apertures above the sputter guns [24]. The sputter guns were operated either at a constant current of 0.5 A, or at a constant power of 215 W. The depositions were carried out at ambient temperatures and at an Ar pressure of 2.3 mTorr, as measured with a capacitance manometer. The film thicknesses were controlled by the translation speeds and the number of loops over the guns according to growth-rate calibrations. All targets were 3 inch in diameter and 0.25 inch thick. The Si target was 99.999% boron-doped and the  $\text{WSi}_2$  target was 99.5% powder-hot-pressed with a density of 8.04 to 8.08 g/cc. The stoichiometry of a sputtered  $\text{WSi}_2$  film as measured using energy-dispersive x-ray (EDX) analyses was  $1.874 \pm 0.118$  Si to

W, slightly off the ideal stoichiometry of two to one. During deposition the guns were programmed to turn on 7 sec before the substrate was moved over and to turn off after a desired thickness was deposited. Additionally, each gun was turned on for 60 sec before a multilayer deposition to clean the targets and stabilize the system. New targets were subjected to a total of 40 min burn-in under the same sputter conditions before being used for deposition.

Periodic  $\text{WSi}_2/\text{Si}$  multilayer test samples were grown and measured using x-ray reflectance. Analysis of the reflectivity was done with the aid of IMD, a computer program for modeling the optical properties of multilayers [25,26]. Reflectivity measurements were made in  $\theta$ - $2\theta$  geometry over the range from  $0 < \theta < 6^\circ$ , using  $\text{Cu-K}\alpha_1$  x-rays with a Ge crystal monochromator and collimating slits. The diffractometer was operated at 1.2 kW with an accuracy of 0.002 deg in  $2\theta$ . A counting time of 1 sec was used at each  $\theta$  increment of 0.005 degrees. The measured data were compared with that calculated using the IMD software for a best fit to determine layer thicknesses and interface parameters. To obtain a more accurate measure of  $\gamma$  (the  $\text{WSi}_2$  to Si ratio), two different  $\text{WSi}_2/\text{Si}$  multilayers were grown on two substrates 25 cm apart under the same growth conditions, with the number of translation loops for  $\text{WSi}_2$  layers differing by a factor of two. The difference in d spacing was then used as  $\text{WSi}_2$  layer thickness for the thinner multilayer. This procedure is justified since  $\text{WSi}_2/\text{Si}$  multilayers have sharp interfaces with little interdiffusion and the Si growth rate in the multilayer scales linearly with deposition time [14,18].

A linear zone-plate structure is defined by Eq. (1), with  $r_n$  defined as the distance between the outer edge of the  $n$ th zone and the optical axis and  $(r_n - r_{n-1})$  as the layer

thickness for that zone. We have chosen an outermost zone of 10 nm,  $\lambda = 0.413 \text{ \AA}$  (30 keV), and  $f = 7.259 \text{ mm}$ , which leads to a maximum number of zones of 750 according to Eq. (1). We chose to grow 728 total layers of  $\text{WSi}_2$  and Si, starting from 10 nm of  $\text{WSi}_2$  and ending at  $\sim 57.74 \text{ nm}$  of Si. A computer program was developed to calculate the thickness of each layer from Eq. (1), the time needed for its growth at certain substrate-moving speed, and the growth-rate correction for that layer. This computer program then compiles a command script for the system control program to execute. The transport system is driven by a microstepping motor with built-in indexing manufactured by Compumotor [27]. Periodic test multilayer samples,  $[\sim 3\text{-nm-WSi}_2/\sim 5\text{-nm-Si}]_{\times 15}$  were grown without any growth-rate correction. Multiple test substrates together with substrates for zone-plate multilayers were loaded on the substrate holder, 25 cm apart, to detect the growth-rate drift at different growing stages of the zone-plate multilayer. The power and voltage readings (current and voltage in constant-power mode) of the sputter-gun power supplies were logged to the computer during the growth.

### **3. Results and discussion**

#### *3.1 Difference between constant-current and constant-power control of the sputter power supply*

When the constant-current mode was used for prolonged multilayer growths, a linear decline of the supply voltage and power was observed in Si and  $\text{WSi}_2$  depositions. Figure 2a shows the power reading of both power supplies for  $\text{WSi}_2$  and Si as a function of growth time during the growth of a zone-plate multilayer at a constant current of 0.5 A. A decrease in power of  $\sim 7.2\%$  for  $\text{WSi}_2$  and  $\sim 7.8\%$  for Si is seen. The decreased power accelerates the decrease of the growth rate in addition to the effect of target usage, since

the growth rate is proportional to the sputter power and geometric factors [28,29]. X-ray results from test samples indicate a decrease in growth rates of over 12% at the end of the zone-plate multilayer growth. A slower drift of the growth rate was confirmed when a constant power of 215 W was used for sputtering. The decrease was ~5% for a similar target usage. The actual decrease in growth rates depends on the condition of the target. In general, the rates decrease more with the target usage. This trend was similar for both  $\text{WSi}_2$  and Si targets. For better stability of growth rates, a constant-power control should be used for prolonged depositions.

### *3.2 Overcoming the deposit flaking problem*

Another problem associated with prolonged multilayer deposition is the flaking of thick deposit from shielding cans, masks and substrate supports. The falling flakes will disturb the magnetron plasma, affect the deposition rate and system stability, even electrically short the sputter gun [18]. We noticed that flaking was most serious on the Si target. Not much flaking was observed from the  $\text{WSi}_2$  deposit. But the flakes falling down from the passing substrate support could still fall onto the  $\text{WSi}_2$  target. Our shield can top, masks, and substrate supports were all made from aluminum. The big difference in thermal expansion coefficients between aluminum and silicon makes it hard for thick Si films to stick firmly on aluminum plates. We found that by roughening the aluminum plates one can enhance the adhesion. We tried also cutting into the aluminum plates to make 1-mm-wide and 1-mm-deep circular grooves to improve adhesion. But it made the flaking problem much worse during a zone-plate multilayer growth. Figure 2b shows the recorded log of the sputtering current of Si for that special run of zone-plate multilayer coating at constant-power mode. The current dropped at ~27 h and fluctuated afterwards,

indicating Si flakes falling onto the target. When the Si flakes fall onto the target, they cause a decrease of secondary electrons, an increase of supply voltage, and a current decrease. They also disturb the sputtering process in a complicated way. These disturbances make the growth-rate unpredictable. For example, x-ray reflectivity measurements for the two test samples grown at  $\sim 21$  h and at the end of the zone-plate multilayer growth shows that the growth rate at the end is higher than that at  $\sim 21$  h. In a normal situation, the rate should be lower. We have tried to use Mo plates as the masking and shielding material; flaking was reduced. Figure 2c shows the current log when Mo plates were used. The darker strips at  $\sim 21$  h in Fig. 2b and at the end of Fig. 2b and 2c are due to test multilayers growths, where the sputter current has a higher on/off frequency. We have found that Si sticks to aluminum foil much better than to aluminum plates, due to the flexibility of the foil. We covered the inside of the shield can and the mask with 1.5-mil aluminum foil and replaced aluminum rods with Si strips to support the zone-plate-multilayer substrates. This practice eliminated completely the flaking problem in our latest zone-plate multilayer growth.

### *3.3 SEM image analyses*

A zone-plate multilayer sample was examined in a SEM. The sample was grown using constant-sputter currents of 0.5 A. The supply power log for this run has been shown in Fig. 2a. The growth-rate correction was determined according to analyses of SEM images in a previous study [18]. In that study, a 470-layer zone-plate multilayer with layer thicknesses varying from 15 to 60 nm was grown using constant-current control and a linear growth-rate correction from 0 to 7.5% over the whole deposition of the  $\sim 11$ - $\mu\text{m}$ -thick multilayer. Although the log of sputter power readings (Fig. 2a) shows

a linear decrease, the analyses from the SEM image indicated a nonlinear growth. The layers at the thin end of the multilayer were thicker and those at the thick end were thinner than expected, indicating an overcorrection at the thin end and undercorrection at the thick end. For the present growth, the correction was readjusted. The thickness for coating each layer was gradually increased from the calculated zone-plate value along a smooth curve, with zero correction for layer 1, ~1% increase for layer 350, ~2.6% for layer 600, and 6.7% for the last layer, layer 728. We will discuss more on this thickness correction later.

For the SEM experiment, the face of the multilayer was glued to another Si substrate and sectioned to  $\sim 1 \times 2 \text{ mm}^2$  pieces using a diamond dicing saw. The side of the cutting was polished carefully and examined in a SEM. Figure 3 shows a SEM image of the cross section of the multilayer. The bright strips are  $\text{WSi}_2$ , and the dark ones are Si. The image shows flat and sharp interfaces of the multilayer. A gradual change in d-spacing is clearly seen. The SEM image was analyzed using image analysis techniques to determine the positions of each layer based on the contrast between neighboring layers. Figure 4 shows the inverse of layer thickness of the measured zone-plate multilayer as a function of layer position. The thinnest layer was put at the position of  $15 \text{ }\mu\text{m}$ , which is the distance from that layer to the optical axis of the zone-plate. The targeted values of the zone-plate structure are also shown for comparison. According to Eq. (1), the inverse of the layer spacing  $1/\Delta r_n$  as plotted at layer position  $r_n$  should be a straight line (for  $\lambda \ll f$ ) with a slope equal to  $-2/\lambda f$ . Figure 4 shows that the measured data are all thinner than the targeted values, presumably due to an initial calibration error of over 3%. The accuracy of SEM scans is  $\sim \pm 4\%$ . Deviation from a straight line for the measured data is

evident. On the lower end of the curve, the data drift downward, indicating a slight over-correction, which makes the layers thicker. In the middle positions, the data are slightly above a straight-line fit (not shown), indicating some undercorrection, which makes the layers thinner than expected.

The sectioned multilayer piece was polished on both faces to a wedge with a desired range for x-ray focusing experiments. A focused line profile with a full-width-at-half-maximum (FWHM) of  $\sim 60$  nm was obtained at an x-ray energy of 19.5 keV using only one multilayer section. This result compares well to our last result of  $\sim 72$  nm line-focusing for a zone-plate multilayer with the thinnest layer thickness of 15 nm [30].

To further improve the zone-plate multilayer performance, we need to understand the growth-rate drift as a function of increasing layer thicknesses. In the following we describe our most recent experiments.

#### *3.4 Growth-rate drifting as measured at different growing stages*

To detect how the growth-rate was changing during the zone-plate multilayer growth, five test multilayers were grown in the same run with a zone-plate multilayer, but at different stages. One was grown at the very start, one at  $\sim 1/3$  of the zone-plate-multilayer growth, one at  $\sim 2/3$ , and the other two at the very end. From the last two test multilayers, the  $\gamma$  was determined. The growths were done under the same growth conditions, except for the last two where the number of substrate-moving loops was doubled for one of them. The sputtering power supplies were controlled in constant-power mode.

Figure 5 shows the normalized d-spacing values obtained from x-ray reflectivity measurements of these periodic samples together with the expected values from the

thickness correction that we used in making the SEM sample showing in Fig. 4. Clearly the growth-rate decreased nonlinearly as the zone-plate multilayer growth progressed. This nonlinearity is in agreement with SEM image analyses. However, the trend of decrease was not what we expected. As seen from the figure, we expected a smooth and accelerated decrease, which is not we see in the measured x-ray data. The result of the last correction has been shown in Fig. 4, where an overcorrection at the end and an undercorrection in the middle of the zone-plate-multilayer growth were observed. This result is in qualitative agreement with the result shown in Fig. 5. At the end of the growth (position 12.43  $\mu\text{m}$ ) the measured x-ray data is higher than that expected from the correction, indicating the actual decrease is less than we expected and the film grown with that correction will be thicker – an overcorrection. For the middle stages of the growth, the reverse is true.

The growth rate is proportional to the sputter power and geometric factors. Since the sputter power was either controlled as constant or decayed linearly, it is thus not directly responsible for the nonlinearity of the growth-rate drift. From purely geometric considerations, the film thickness depends on the geometry and area of the sputter source and its emission characteristics [31,32]. For the emission characteristic, each point on the erosion surface of the target can be assumed to be a point source, with the highest emission along the normal to the surface. After a complete set of zone-plate and test multilayer growths, the erosion depth of the target was observed to increase by  $\sim 1$  mm. This increases the distance from the target to the substrate and decreases the growth rate. However, without a change in the erosion profile, this 1 mm difference would cause only an almost linear decrease of less than 1% of the film thickness in our system according to

Eq. 1 in Ref. 31, which relates the film thickness from a ring source to the mass of emitted material, the radius of source ring, the source to substrate distance, and the position on the substrate. The real influence comes from the change in the erosion profile. For a new target, the erosion is very shallow and most atoms are sputtered upward towards the substrate. With increasing target usage, the erosion groove becomes deeper and its cross section looks like a cup. The atoms sputtered from the side surface of the erosion groove will have less projection to the substrate compared to that from a flat surface. The growth rate thus depends very sensitively to the erosion profile in a nonlinear manner. Clearly, more studies in this regard are needed for future fabrications of zone-plate multilayers.

From x-ray reflectivity measurements of the last two test samples, we found that the thickness of  $\text{WSi}_2$  has decreased by 5.3% and Si by 6.0% compared to the values measured at the start of zone-plate multilayer growth.

#### **4. Summary**

We have succeeded in growing a nanostructured depth-graded multilayer for linear zone-plate applications to focus hard x-rays. We found that it is better to use constant-power control to grow this kind of thick multilayers. We have found practical means to overcome the Si deposit flaking problem in an upward sputtering geometry. Detailed studies of periodic samples with x-ray reflectivity measurements and image analyses of SEM scans of zone-plate multilayers have demonstrated a nonlinear growth rate decreases with growth time. This nonlinear behavior is explained from geometric considerations of sputtered atoms. A sectioned and polished zone-plate multilayer has

been tested in a synchrotron nanofocus experiment. A line-focus of ~60 nm FWHM was achieved at an x-ray energy of 19.5 keV.

### **Acknowledgments**

We thank R. Khachatryan, M. Wieczorek, and G. Czop for technical assistance and M. Kirk and R. Koritala for help of EDX analyses, all from Argonne National Laboratory. We thank M. A. Zurbuchen for his earlier contribution of SEM work. This work is supported by the U. S. Department of Energy, Office of Science, Office of Basic Energy Sciences, under Contract No. W-31-109-ENG-38.

### **References**

1. J. Kirz, *J. Opt. Soc. Am.* 64 (1974) 301.
2. E. Spiller, *Soft X-ray Optics*, SPIE Optical Engineering Press, Bellingham, WA, 1994.
3. J. Als-Nielsen and D. McMorrow, *Elements of Modern X-ray Physics*, John Wiley & Sons, New York, 2001.
4. A. A. Krasnoperova, J. Xiao, F. Cerrina, E. Di Fabrizio, L. Luciani, M. Figioment, M. Gentill, W. Yun, B. Lai, and E. Gluskin, *J. Vac. Sci. Technol. B* 11 (1993) 2588.
5. M. Peuker, *App. Phys. Lett.* 78 (2001) 2208.
6. W. Chao, E. Anderson, G. P. Denbeaux, B. Harteneck, J. A. Liddle, D. L. Olynick, A. L. Pearson, F. Salmassi, C. Y. Sony, and D. T. Attwood, *Opt. Lett.* 28 (2003) 2019.
7. T.W. Barbee, *Opt. Eng.* 25 (1986) 898.
8. R. M. Bionta, E. Ables, O. Clamp, O. D. Edwards, P. C. Gabriele, K. Miller, L. L. Ott, K. M. Skulina, R. Tilley, and T. Viada, *Opt. Eng.* 29 (1990) 576.

9. N. Kamijo, Y. Suzuki, M. Awaji, A. Takeuchi, H. Takano, T. Ninomiya, S. Tamura, and M. Yasumoto, *J. Synchrotron Rad.* 9 (2003) 182.
10. J. A. Thornton, *J. Vac. Sci. Technol. A* 4 (1988) 3059.
11. H. C. Kang, G. B. Stephenson, C. Liu, R. Conley, A. T. Macrander, J. Maser, S. Bajt, and H. N. Chapman, *Proc. SPIE* 5537 (2004) 127.
12. J. Maser, G. B. Stephenson, S. Vogt, W. Yun, A. T. Macrander, H. C. Kang, C. Liu, and R. Conley, *Proc. SPIE* 5539 (2004) 194.
13. H. C. Kang, G. B. Stephenson, C. Liu, R. Conley, A. T. Macrander, J. Maser, S. Bajt, and H. N. Chapman, *Appl. Phys. Lett.* 86 (2005) 151109.
14. C. Liu, R. Conley, A. T. Macrander, T. Graber, Ch. Morawe, C. Borel, and E. M. Dufresne, *Proc. SPIE* 5537 (2004) 154.
14. A. I. Fedorenko et al., *Proc. SPIE* 2453 (1995) 15.
15. R. Senderak et al., *J. Appl. Phys.* 81 (1997) 2229.
16. D. L. Windt, F. E. Christensen, W. W. Craig, C. Hailey, F. A. Harrison, M. Jimenez-Garate, R. Kalyanaraman, and P. H. Mao, *J. Appl. Phys.* 88 (2000) 460.
17. C. Liu, R. Conley, A. T. Macrander, J. Maser, H. C. Kang, M. A. Zurbuchen, and G. B. Stephenson, to be published.
18. F. Eriksson, G. A. Johansson, H. M. Hertz, E. M. Gullikson, U. Kreissig, and J. Birch, *Opt. Lett.* 28 (2003) 2494.
19. Ch. Morawe, E. Ziegler, J. –Ch. Peffen, I. V. Kozhevnikov, *Nucl. Instr. And Meth.* A493 (2002) 189.
20. V. V. Martynov, Yu. Platonov, A. Kazimirov, D. H. Bilderback, *AIP Conf. Proc.* 705 (2004) 697.

21. S. Berg and I. Katardjiev, Surf. Coat. Technol. 84 (1996) 353.
22. F. Eriksson, private communication, May 2005.
23. C. Liu, R. Conley, and A. T. Macrander, J. Vac. Sci. Technol. A 22 (2004) 1610.
25. D. L. Windt, Computers in Physics, 12 (1998) 360.
26. D. L. Windt, 2004, <http://cletus.phys.columbia.edu/~windt/idl/>.
27. Compumotor Division, Parker Hannifin Corp., Rohnert Park, CA 94928.
28. S. Maniv and W. D. Westwood, J. Vac. Sci. Technol. 17 (1980) 743.
29. M. Bhushan, J. Vac. Sci. Technol. A 5 (1987) 2829.
30. H. C. Kang, G. B. Stephenson, C. Liu, R. Conley, A. T. Macrander, J. Maser, unpublished (2005).
31. S. Swann, Vacuum 38 (1988) 791.
32. C. Liu, L. Assoufid, R. Conley, A. T. Macrander, G. E. Ice, and T. Z. Tischler, Opt. Eng. 42 (2003) 3622.

## FIGURE CAPTIONS

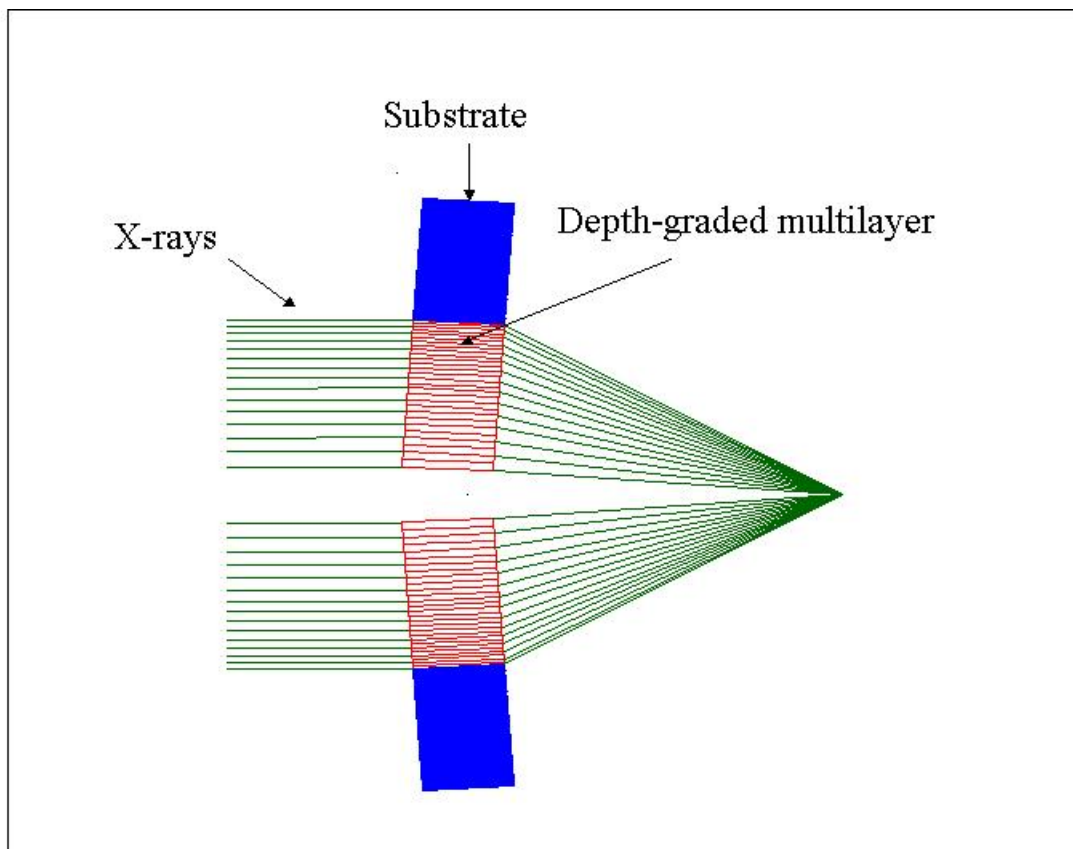
Fig. 1 Schematic of a linear zone plate concept. A pair of sectioned depth-graded multilayers is positioned and tilted at an optimum angle to focus the x-rays into a fine line.

Fig. 2 Computer logs for a) supply power of both power supplies during a zone-plate multilayer growth at a constant-current control of 0.5 A, the power supply for  $\text{WSi}_2$  had slightly higher readings, b) supply current readings for Si during a zone-plate multilayer growth at a constant-power control of 215 W, c) same as b) but with much less flaking, see text.

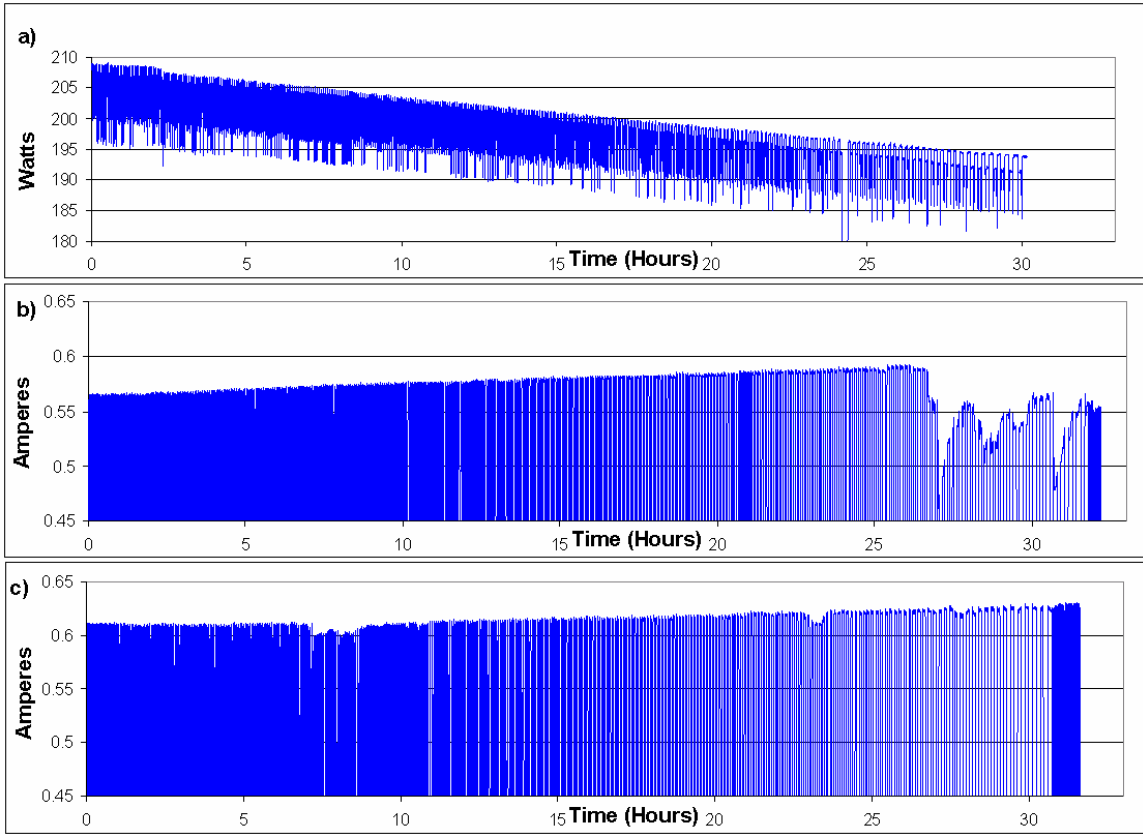
Fig. 3 Cross-section SEM image of a  $\text{WSi}_2/\text{Si}$  zone-plate multilayer structure. The bright strips are  $\text{WSi}_2$ , and the dark ones are Si. The substrate is on the left side of the image. The inserts are enlarged views.

Fig. 4 Measured inverse layer thicknesses versus layer position compared to the targeted values. The measured thicknesses are all thinner than the targeted values. The measured data deviate slightly from a straight line on the lower end and in the middle positions. Two layer position scales are used to reveal the relative relationship between measured and targeted results at the beginning, middle, and end of growth.

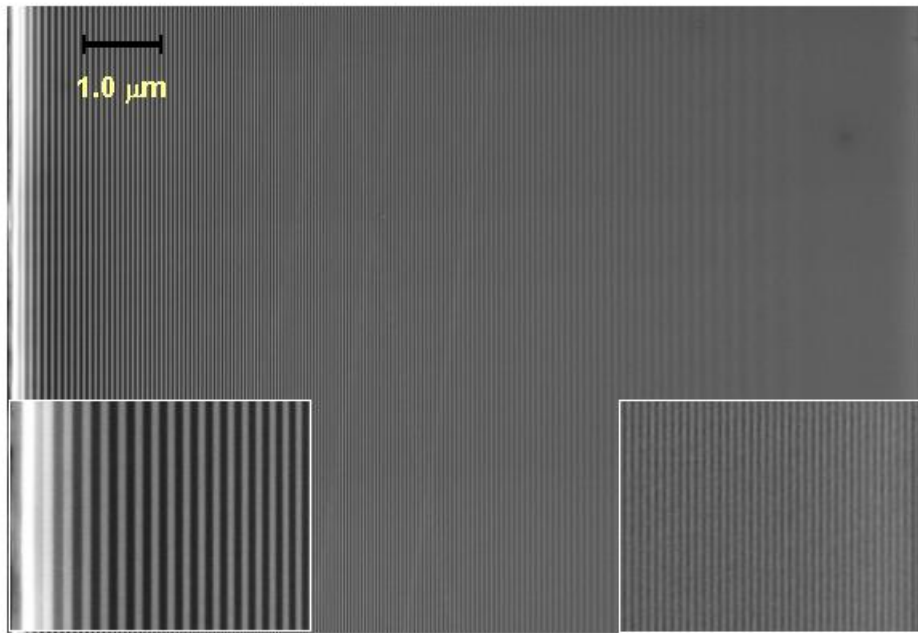
Fig. 5 Normalized d spacing of four periodic test samples grown at different growth stages of a zone-plate multilayer. The lines connecting the data are a guide to the eye. The expected values from last thickness correction we used to grow the sample shown in Fig. 4 is also plotted for comparison.



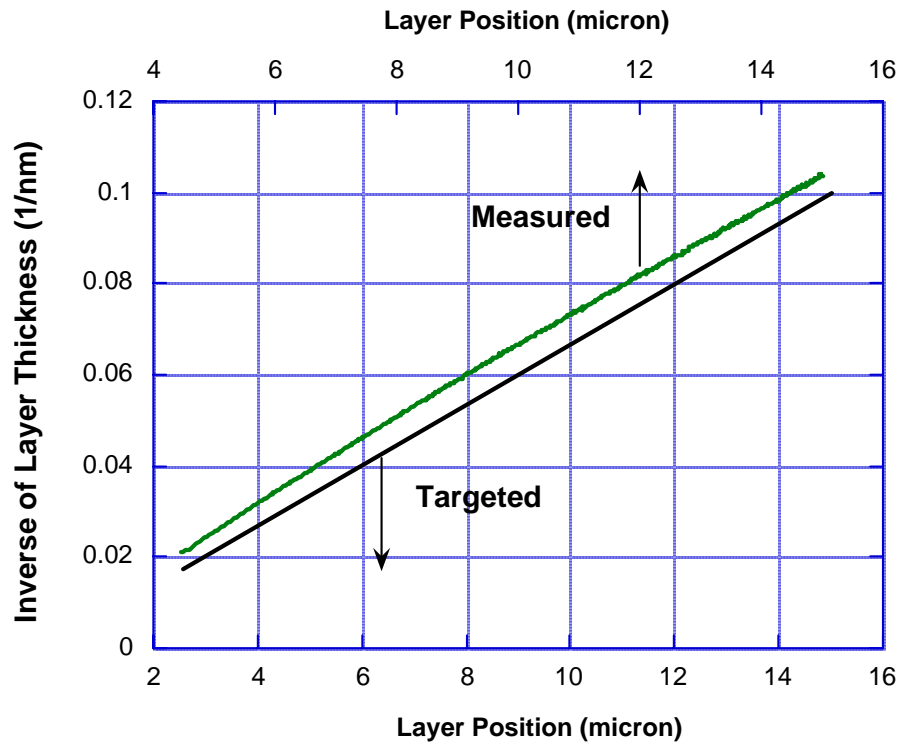
LIU, FIGURE 1



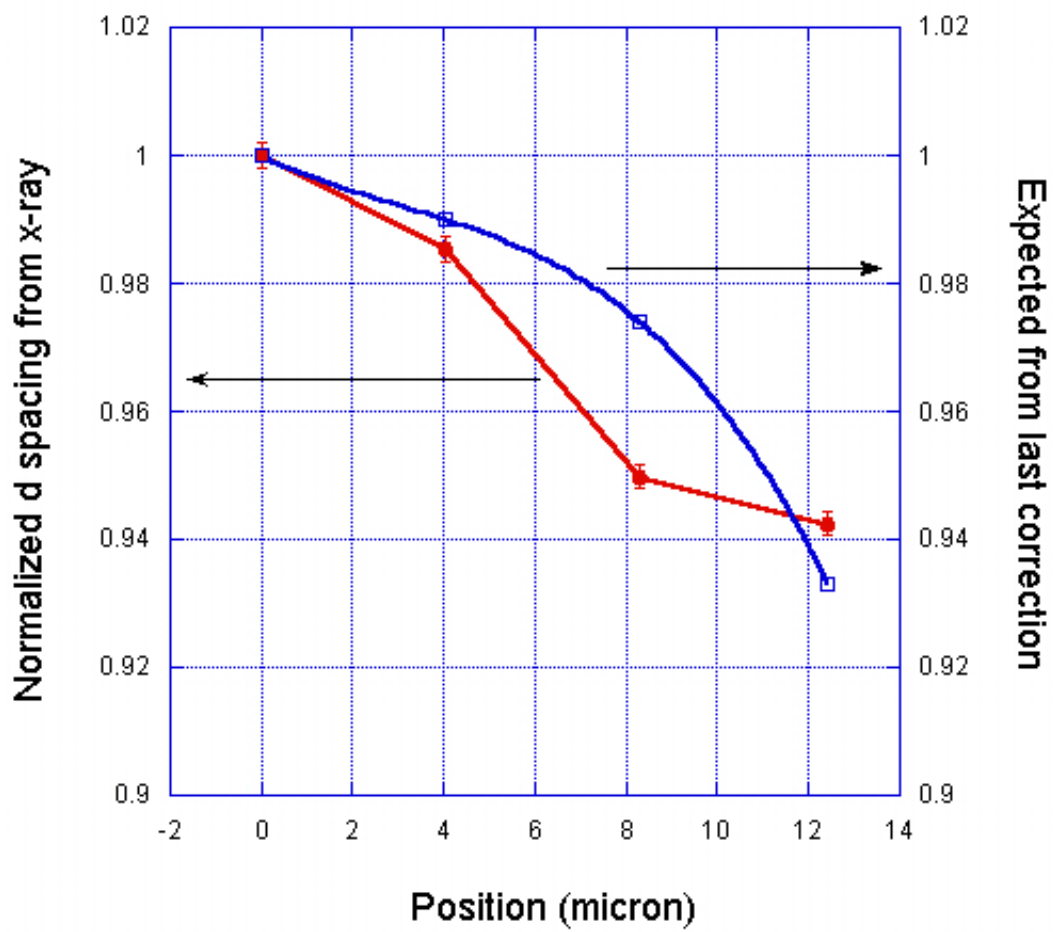
LIU, FIGURE 2



LIU, FIGURE 3



LIU, FIGURE 4



LIU, FIGURE 5